Eur. Phys. J. Appl. Phys. **50**, 10601 (2010)
DOI: 10.1051/epjap/2010011

THE EUROPEAN PHYSICAL JOURNAL APPLIED PHYSICS

Regular Article

Symmetry-induced perfect transmission and inverse magnetoresistance in cascade junctions of ferromagnet and semiconductor

R.L. Zhang, J.S. Zhang, D. Li, J. Li, and R.W. Peng[a]

National Laboratory of Solid State Microstructures and Department of Physics, Nanjing University, Nanjing 210093, P.R. China

Received: 16 June 2009 / Received in final form: 9 November 2009 / Accepted: 17 December 2009
Published online: 26 February 2010 –

Abstract. Within the Landauer framework of ballistic transport, we theoretically investigate spin-dependent resonant transmission and magnetoresistance in symmetric cascade junctions of ferromagnetic metal (FM) and semiconductor (SC). It is shown that spin-up and spin-down electrons possess different bandgap structures against the Rashba spin-orbit wave vector. Due to the mirror symmetry, multiple spin-dependent perfect transmissions of electrons can be obtained within the bandgap, thereafter, spin polarization has multiple reversals. Around each resonant wave vector, high spin polarization is achieved and the electrical conductance comes from one kind of spin electrons. The resonant transmissions originate from the spin-dependent quasi-bound states at energies above the potential barriers, which are demonstrated by the electronic charge distributions in the system. Furthermore, if we change the magnetization of FM in the centre of the junctions, inverse magnetoresistance can be observed. The investigations may have potential applications in spin filters and spin switches.

1 Introduction

Motivated by the pioneer work of Datta and Das [1], much attention has been paid to the spin-polarized transport in spin field-effect transistor. In such a system, ferromagnetic metals (FMs) are used as spin injector and detector, and in between there is a semiconductor (SC) to tune the spin precession. The Rashba spin-orbit coupling (SOC) in semiconductor can lead to different spin precessions for spin-up and spin-down electrons [2–8]. The strength of Rashba SOC can be controlled by a gate voltage applied on the semiconductor. It has been reported in experiments that injection of spin-polarized current in FM/SC systems is being constantly improved at room temperature [9–12]. Recently, quantum spin-valve, spin-switching and spin-filtering effects have been found in the FM/SC/FM junction [13–19]. These investigations make it possible to manipulate the spin-polarized transport by designing FM/SC junctions, and use them as spintronic devices.

On the other hand, it is known that in quantum confined systems, the bound states at energies above the potential wells (or barriers) can induce resonant transmissions within the electronic bandgap [20–23]. By designing various potential, wavefunctions and electronic properties of the materials can be tuned, which can be applied in energy bandgap engineering. Meanwhile in random polymer systems, the internal symmetry can lead to resonant transmission of electrons. This phenomenon was first predicted by Dunlap et al. in one-dimensional random-dimer (RD) model [24] and has been experimentally demonstrated in RD GaAs-AlGaAs superlattice [25]. Similar resonant phenomena have been found in various correlated disorder systems [26,27]. Physically, the internal symmetry induces the extended electronic states, thereafter, resonant transmission of electrons is observed in those systems. As an analog, the internal symmetry has induced perfect transmissions of electromagnetic waves in dielectric microstructures, which has achieved applications on the wavelength division multiplexing system [28,29].

In this work, we study how the mirror symmetry affects the spin-dependent transport of electrons in FM/SC cascade junctions. It is shown that multiple perfect transmissions for spin-up or spin-down electrons are found within the bandgap against the Rashba spin-orbit wave vector. Both the wave vector and the mode number of resonant transmissions therein can be tuned. Around resonant wave vector, high spin polarization is achieved and electrical conductance is contributed only by single spin state. The resonant transmissions originate from the spin-dependent quasi-bound states at energies above the potential barriers. Furthermore, inverse magnetoresistance is found in the system. This paper is organized as following.

[a] e-mail: rwpeng@nju.edu.cn

In Section 2, we present the analytical analysis of spin-dependent transport in the FM/SC cascade junctions with a mirror symmetry based on the transfer matrix method. In Section 3, the spin-dependent transmission, spin polarization and the electric conductance are calculated numerically. The physical origin of the spin-dependent resonant phenomena is discussed based on the electronic charge distribution of the system. In Section 4, the effect of inverse magnetoresistance is discussed in the SCJ. A brief summary is given in Section 5.

2 The theoretical analysis

In the Landauer formalism of ballistic transport [30], we consider spin-dependent transport of electrons through a FM/SC symmetric cascade junction (SCJ) constructed as

$$S(m,\ n) = (FM/SC)^m (SC)^n (SC/FM)^m, \qquad (1)$$

where m and n are the repeated numbers of the units (as schematically shown in Fig. 1a). Figure 1b plots the conduction band diagram in the SCJ of $S(5,\ 0)$. To achieve the SCJ, one can carve grooves on top of a near-surface 2DEG formed in semiconductor heterostructures, and fill in the grooves by deposing an FM material. The SCJ quasi-one-dimensional waveguide can be obtained by confining in the z-direction. Suppose that spin transport along the x-axis in a quasi-one-dimensional waveguide, which is composed of the SCJ shown in equation (1). And electrons are confined in the y-direction by an asymmetric quantum well in the semiconductor, where the Rashba SOC exists. In practice, one may tune the Rashba SOC via spatially distributed gates, which can be made on top of semiconductor by micro-fabrication technique, for example, E-beam lithography [31]. In each FM layer, a Stoner-Wohlfarth-like model of magnetization is exploited, then the energy offset between the spin-up and spin-down bands can be set as the exchange splitting energy Δ. The orientation of the magnetization is along the z-direction. Based on the one-band effective-mass approximation, the Hamiltonians in the FM and SC regions can be written as

$$\hat{H}_f = \frac{1}{2}\hat{p}_x \frac{1}{m_f^*}\hat{p}_x + \frac{1}{2}\Delta\sigma_z, \qquad (2)$$

and

$$\hat{H}_s = \frac{1}{2}\hat{p}_x \frac{1}{m_s^*}\hat{p}_x + \frac{1}{2\hbar}\sigma_z[\hat{p}_x\alpha_R + \alpha_R\hat{p}_x] + \delta E, \qquad (3)$$

respectively. Here m_f^* and m_s^* are the effective masses of electrons in the FM and SC, respectively. σ_z denotes the spin Pauli matrices, α_{R} is the spin-orbit Rashba parameter, and δE is the conduction-band mismatch between SC and FM. It should be noted that, because of the conduction-band mismatch in a realistic FM/SC junction, increasing the spin polarization in FM helps little to increase spin-injection rate unless the spin polarization in FM approaches 100% [32]. Due to the fact that the Hamiltonians shown in equations (2) and (3) are spin diagonal, the electronic eigenstates in the system have the form of $|\Psi_\uparrow\rangle = [\psi_\uparrow(x),\ 0]$ and $|\Psi_\downarrow\rangle = [0,\ \psi_\downarrow(x)]$. By using the continuous conditions, the transfer matrix from FM to SC layers has the form of

$$T_{FS} = \frac{1}{2K_s}\begin{pmatrix} \eta_{\sigma+} & \eta_{\sigma-} \\ \eta_{\sigma-} & \eta_{\sigma+} \end{pmatrix}, \qquad (4)$$

while the transfer matrix from SC to FM layers can be expressed by:

$$T_{SF} = \frac{1}{2\mu k_{F\sigma}^f}\begin{pmatrix} \eta_{\sigma+} & -\eta_{\sigma-} \\ -\eta_{\sigma-} & \eta_{\sigma+} \end{pmatrix}. \qquad (5)$$

Here

$$K_s = k_{F\sigma}^s + \lambda_\sigma K_R = \sqrt{(K_R)^2 + \mu(k_{F\sigma}^f)^2 - \frac{2m_s^*}{\hbar^2}(\delta E - \frac{1}{2}\lambda_\sigma \Delta)},$$

which can be achieved by energy conservation in the system, and $\eta_{\sigma\pm} = (K_s \pm \mu k_{F\sigma}^f)$. $k_{F\sigma}^s$ and $k_{F\sigma}^f$ are the Fermi wave vectors in the SC and FM regions, respectively, $\mu = m_s^*/m_f^*$, $K_R = m_s^*\alpha_R/\hbar^2$, and $\lambda_{\uparrow,\downarrow} = \pm 1$. The electronic propagation within the FM layer can be described by matrix T_F,

$$T_F = \begin{pmatrix} e^{ik_{F\sigma}^f d_f} & 0 \\ 0 & e^{-ik_{F\sigma}^f d_f} \end{pmatrix}, \qquad (6)$$

and the electronic propagation within the SC layer can be written as

$$T_S = \begin{pmatrix} e^{ik_{F,+\sigma}^s d_s} & 0 \\ 0 & e^{-ik_{F,-\sigma}^s d_s} \end{pmatrix}, \qquad (7)$$

where $+\sigma$ (or $-\sigma$) indicates the same (or opposite) spin state with σ. d_f is the thickness of each FM layer, and d_s is the thickness of each SC layer. In the following calculations, the thicknesses of FM and SC have been set as $d_f = 1$ nm and $d_s = 0.1$ μm, respectively. By this assumption, the length of the whole system is about several micrometers, and we can carry out theoretical investigation in the Landauer formalism of ballistic transport. Therefore, the whole system is represented by a product matrix M, relating the incident and reflection waves to the transmission wave. The transmission coefficient of the electron with the spin state σ through the whole SCJ can be described by:

$$T_\sigma = \left(\frac{k_{F\sigma}^{f,L}}{k_{F\sigma}^{f,R}}\right)\left|\frac{1}{M_{22}}\right|^2, \qquad (8)$$

where $k_{F\sigma}^{f,L}$ and $k_{F\sigma}^{f,R}$ are the Fermi wave vectors in the 1st and the Nth FM electrodes, respectively. Here N is the total number of units in the SCJ. $M_{ij}(i,j = 1,\ 2)$ are the elements of the product matrix M.

It is necessary to pay attention to the product transfer matrix through the SCJ, i.e., M. In

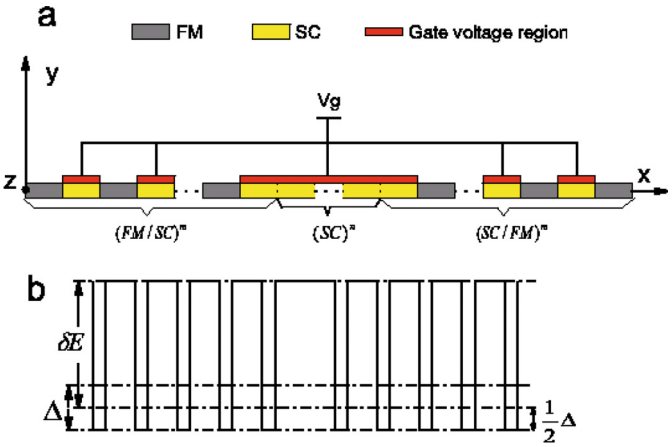

Fig. 1. (Color online) (a) shows schematically a FM/SC symmetric cascade junction (SCJ) given by equation (1), where a gate voltage (V_g) tunes the Rashba spin-orbit coupling. (b) Conduction band diagram in the SCJ of $S(5,\ 0)$.

the SCJ, the FM and SC layers are arranged as "$(FM/SC)^m(SC)^n(SC/FM)^m$". If we define the transfer matrices M_L and M_R as

$$M_L = T_{SF}T_ST_{FS}T_F = \begin{pmatrix} u & v \\ w & x \end{pmatrix}, \tag{9}$$

and

$$M_R = T_FT_{SF}T_ST_{FS} = \begin{pmatrix} u & -w \\ -v & x \end{pmatrix}, \tag{10}$$

respectively, the product transfer matrix of SCJ of $S(m,\ n)$ can be written as

$$M(m) = M_LM(m-1)M_R = \begin{pmatrix} G_m & H_m \\ -H_m & F_m \end{pmatrix}, \tag{11}$$

where $G_m = u^2G_{m-1} - 2uvH_{m-1} - v^2F_{m-1}$, $H_m = -wuG_{m-1}+(wv+xu)H_{m-1}+xvF_{m-1}$, $F_m = -w^2G_{m-1}+2wxH_{m-1} + x^2F_{m-1}$ for $m > 1$. In the case of $m = 1$, $G_1 = \eta^2_{\sigma+}e^{ik^s_{F,+\sigma}(n+2)d_s} - \eta^2_{\sigma-}e^{-ik^s_{F,-\sigma}(n+2)d_s}$, $H_1 = \eta_{\sigma+}\eta_{\sigma-}e^{ik^s_{F,+\sigma}(n+2)d_s} - \eta_{\sigma+}\eta_{\sigma-}e^{-ik^s_{F,-\sigma}(n+2)d_s}$, and $F_1 = \eta^2_{\sigma+}e^{-ik^s_{F,-\sigma}(n+2)d_s} - \eta^2_{\sigma-}e^{ik^s_{F,+\sigma}(n+2)d_s}$.

Because there exists mirror symmetry in the SCJ, we can easily find the conditions for the perfect transmission, i.e., once

$$|M_{22}| = |F_m| = 1 \tag{12}$$

is satisfied, perfect transmissions can be obtained in the SCJ. Here the magnetizations in ferromagnetic layers are in parallel alignment. It should be mentioned that equation (12) can be generally used in the FM/SC cascade junctions with a mirror symmetry. Interestingly, the SCJ has several advantages in tuning perfect transmissions as following. (i) The bandgap for spin-up (or spin-down) electrons is achieved because of the substructures of $(FM/SC)^m$ and $(SC/FM)^m$ in the SCJ. (ii) An internal symmetry exists in the structure, which is expected to induce the perfect transmissions. And the perfect transmissions are spin-dependent. The central parts $(SC)^n$ in the SCJ can tune the number and the wave vector of the perfect transmission peaks due to the phase modulation of electronic wavefunctions. (iii) The quality factor of perfect transmission peaks will be enhanced by increasing the number of the substructures, i.e., $(FM/SC)^m$ and $(SC/FM)^m$, due to multiple scatterings of electrons in the substructures.

Once the spin-dependent transmission coefficient T_σ is achieved, the spin polarization (P) and the conductance (G) [30] of the system can be achieved by:

$$P = (T_\uparrow - T_\downarrow)/(T_\uparrow + T_\downarrow) \tag{13}$$

and

$$G = (e^2/h)(T_\uparrow + T_\downarrow), \tag{14}$$

respectively.

Usually the spin polarization in a tunnel junction can form the tunneling magnetoresistance (TMR). In order to evaluate TMR in the SCJ, we change the magnetization of FM in the centre of SCJ. Then the TMR can be defined as

$$TMR = (G_{\uparrow\uparrow} - G_{\uparrow\downarrow})/G_{\uparrow\uparrow}, \tag{15}$$

where $G_{\uparrow\uparrow}$ and $G_{\uparrow\downarrow}$ represent the tunnel conductance of the SCJ for parallel and antiparallel alignments of the magnetizations in ferromagnetic layers, respectively.

3 The resonant transmission in SCJs

We have calculated the spin-dependent transmission coefficient as a function of Rashba spin-orbit wave vector in the FM/SC SCJs for parallel magnetization. Figures 2a–2c show the transmission spectra in the SCJs of $S(5, n)$ with different n. There are several interesting features. First, due to the substructure of $(FM/SC)^5$ and $(SC/FM)^5$ in the SCJ, there is a spin-dependent bandgap structure against the Rashba spin-orbit wave vector. Second, there exist perfect transmission peaks in the bandgap for spin-up or spin-down electrons. However, the resonant wave vectors for spin-up and spin-down electrons are separated. Third, the central part $(SC)^n$ determines the peak number and the wave vector of perfect transmission peaks in the bandgap for each spin state of electrons. We find that more and more perfect transmission peaks for spin-up or spin-down electrons appear in the bandgap by increasing n. For example, there is one peak for spin-up or spin-down electrons in the bandgap when $n = 0$ (as shown in Fig. 2a). There are two peaks for spin-up or spin-down electrons in the bandgap when $n = 4$ (as shown in Fig. 2b). And three peaks for spin-up or spin-down electrons appear in the bandgap when $n = 8$ (as shown in Fig. 2c). Physically, with increasing the length of SC channel in the centre of the SCJ, phase shift for each spin state is enlarged when the Rashba SOC strength is modulated. As a result, more transmission peaks lie in the bandgap in the SCJ of $S(m, n)$.

The spin-polarization can be tuned by changing both the strength of Rashba SOC and the length of SC channel in the centre of the SCJ. Figures 2d–2f present the spin

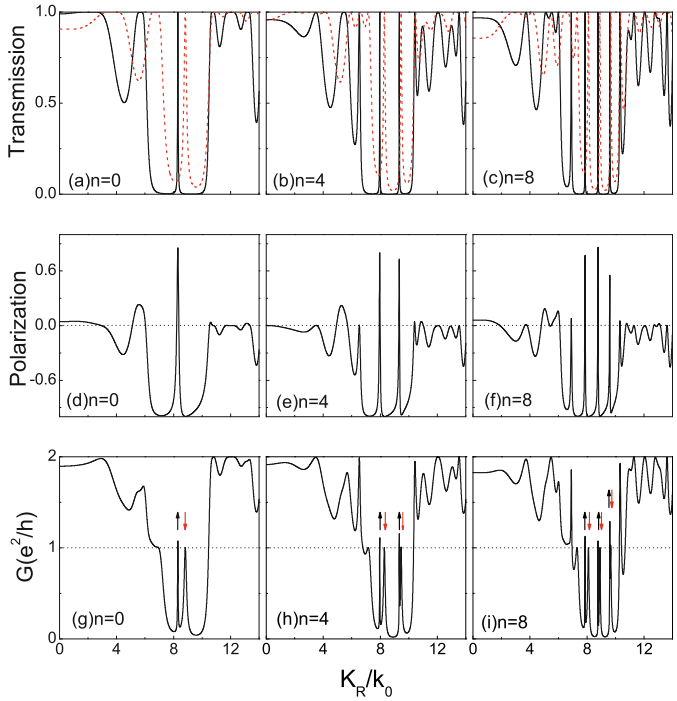

Fig. 2. (Color online) Illustrate the spin-dependent transmission coefficients, the spin polarization, and the conductance (G) as a function of the Rashba spin-orbit wave vector in the SCJ of $S(5,\ n)$ with different n, respectively. For transmission coefficients: (a) $n = 0$, (b) $n = 4$ and (c) $n = 8$. The black solid line corresponds to spin-up electrons, and the red dashed line corresponds to spin-down electrons. For the spin polarization: (d) $n = 0$, (e) $n = 4$ and (f) $n = 8$. And for the conductance: (g) $n = 0$, (h) $n = 4$ and (i) $n = 8$, where the arrow implies the conductance peak contributed by spin-up ($\uparrow$) or spin-down ($\downarrow$) electrons. In all calculations in this work, we assume $m_s^* = 0.036m_e$, $m_f^* = m_e$, and m_e is the free electron mass. The Fermi wave vectors for spin-up and spin-down electrons are set as $k_{F\uparrow} = 0.44 \times 10^8$ cm^{-1} and $k_{F\downarrow} = 1.05 \times 10^8$ cm^{-1}, respectively. The conduction-band mismatch between the SC and FM is $\delta E = 2.4$ eV. All these calculated parameters are reasonable for Fe and InAs-based heterostructures [15,16]. The thicknesses of FM and SC have been set as $d_f = 1$ nm and $d_s = 0.1$ μm, respectively. And $k_0 = 1 \times 10^5$ cm^{-1}, which can be reached in experiments.

polarization against Rashba spin-orbit wave vector in the SCJs of $S(5, n)$ with different n. Obviously, the spin polarization can be changed alternatively from positive to negative when the Rashba spin-orbit wave vector is varied. Around resonant wave vectors, high spin polarization has been observed and the spin polarization has been reversed (as shown in Figs. 2d–2f). This feature originates from the fact that resonant wave vectors are spin-dependent (as shown in Figs. 2a–2c). On the other hand, because more and more spin-dependent transmission peaks appear by increasing n in the SCJ, multiple reversals of spin polarization happen in the bandgap (as shown in Figs. 2e–2f). Consequently, the spin polarization reversal and the reversal times for tunneling electrons can be modulated by tuning the length of SC channel in the center of the SCJ.

It is worthwhile to study the electrical conductance of the FM/SC SCJ. As shown in Figures 2g–2i, there exist conductance peaks within the bandgap against the Rashba spin-orbit wave vector in the SCJs of $S(5, n)$ with different n. The electrical conductance within the bandgap is about e^2/h at each resonant wave vector. As we have known, resonant wave vectors are spin-dependent in $S(5, n)$. At the resonant energy of spin-up electron, the transmission for spin-down electron is close to zero. While at the resonant energy of spin-down electron, the transmission for spin-up electron is almost zero (as shown in Figs. 2a–2c). As a result, the electrical conductance around the resonant wave vector comes mainly from one kind of spin electrons. Then fully spin-polarized conductance with the value of e^2/h can be observed within the bandgap. On the other hand, more and more peaks with about e^2/h appear in the bandgap when n increases (shown in Figs. 2g−2i). Interestingly, the conductance peaks contributed by spin-up or spin-down electrons appear alternately in the bandgap. For instance, the $(2i - 1)$th conductance peak mainly comes from the spin-up electron, and the $(2i)$th conductance peak mainly comes from the spin-down electron in the SCJ of $S(5, n)$. Here $i = 1$ in the case of $S(5,\ 0)$ (as shown in Fig. 2g), $i = 2$ in the case of $S(5,\ 4)$ (as shown in Fig. 2h), and $i = 3$ in the case of $S(5,\ 8)$ (as shown in Fig. 2i). These features may have potential applications in the designing of spin filters.

In order to understand the behavior of spin-up and spin-down electrons clearly, the electronic charge distributions in the SCJ have been studied. Figure 3 plots the electronic charge distributions in the SCJ of $S(5,\ 0)$ at different Rashba spin-orbit wave vectors. As discussed above, there is a transmission peak for spin-up or spin-down electrons in the bandgap of $S(5,\ 0)$ (as shown in Fig. 2a). The resonant modes for spin-up and spin-down electrons in the bandgap are at the wave vectors of $K_{R\uparrow} \cong 8.30k_0$ and $K_{R\downarrow} \cong 8.82k_0$, respectively. For the spin-up electron at $K_{R\uparrow}$, the electronic charge is almost symmetrically distributed (as shown in Fig. 3a and its inset). It is obvious that the injected spin-up electrons can transport through the whole SCJ. The transmitted wave has the same intensity as the incident wave does, thereafter, the transmission of spin-up electron becomes perfect at the wave vector of $K_{R\uparrow}$. But differing with the extended states, some maxima of the wave envelope locate at the center of the SCJ. The wave function of the spin-up resonant mode (shown in Fig. 3a and its inset) exhibits the typical feature of the bound states at energies above the potential barriers [20]. While for the spin-down electron at $K_{R\uparrow}$, the electronic charge distribution decays exponentially (as shown in Fig. 3b), which presents the feature of the localized states. Therefore, the injected spin-up electron at $K_{R\uparrow}$ can propagate through the whole SCJ, which corresponds to the quasi-bound state at energies above the potential barriers for spin-up electron. However, the spin-down electron at $K_{R\uparrow}$ cannot propagate in the system, which corresponds to the localized state for spin-down electron. The opposite case is that the localized state is for spin-up electron, but the quasi-bound state at energies above the potential

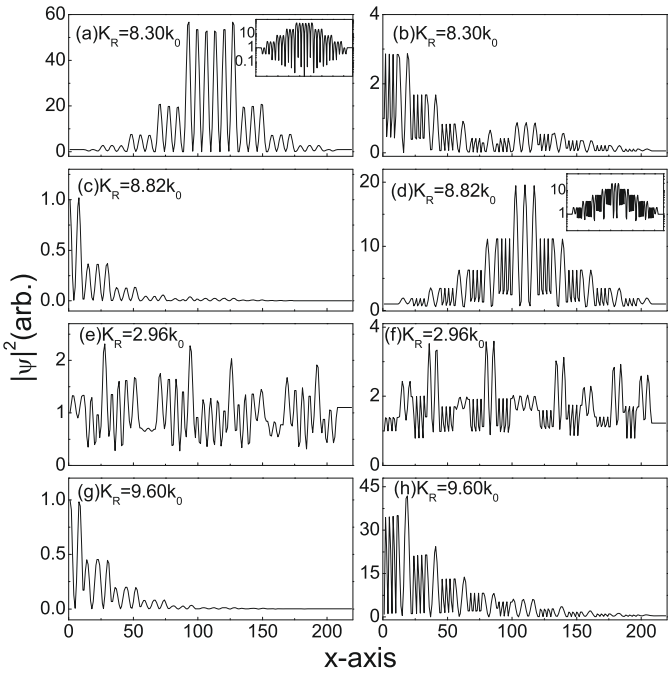

Fig. 3. Shows the spin-dependent electronic charge distributions in the SCJ of $S(5,\ 0)$ when the Rashba spin-orbit wave vector K_R is different. In the case of $K_R = 8.30k_0$: (a) spin-up electrons and (b) spin-down electrons. In the case of $K_R = 8.82k_0$: (c) spin-up electrons and (d) spin-down electrons. In the case of $K_R = 2.96k_0$: (e) spin-up electrons and (f) spin-down electrons. In the case of $K_R = 9.60k_0$: (g) spin-up electrons and (h) spin-down electrons, respectively. In the insets of 3a and 3d, y-axis is logarithmic scale.

barriers for spin-down electron. For example, at $K_{R\downarrow}$, the spin-down electron can propagate through the whole SCJ (as shown in Fig. 3d), while spin-up electron cannot propagate in the system (as shown in Fig. 3c). We have also plotted the extended states for both spin-up and spin-down electrons when the wave vector is in the band and electrons can propagate in the system (as shown in Figs. 3e and 3f). Meanwhile, the localized states for both spin-up and spin-down electrons can be observed when the wave vector lies in the electronic bandgap and both types of electron cannot propagate (as shown in Figs. 3g and 3h). All these electronic states indeed determine the quantum transport in the SCJ. This implies that by constructing the microstructure, spin-dependent potential can be designed and electronic properties of the materials can be tailored, which may be applied in energy bandgap engineering.

Furthermore, we would like to mention that in a real FM/SC system, there usually exists Schottky barrier at the interface. The Schottky barrier provides a natural tunnel barrier between a metal contact and a SC, which is helpful for the injection of spin polarized electrons [9–12]. Meanwhile, the Schottky barrier has a strong effect on the spin-transmission probabilities, which may lead to sharper transmission peaks [4,5,15,16].

4 The inverse magnetoresistance in SCJs

It is well known that there is tunnel magnetoresistance (TMR) in magnetic tunnel junctions (MTJs) consisting of two thick FM layers and a thin insulator. According to Julliere's model [33], TMR in the MTJ is related to the spin polarization of the electrodes independently and usually it is positive. However, inverse TMR has been observed experimentally in the MTJs [34–36], which means that the conductance in the antiparallel magnetic configuration is higher than that in the parallel configuration. And inverse (or negative) magnetoresistace has also been found in fractal Pb thin film on Si(111) [37]. Both normal and inverse TMRs have been observed in the nanowires consisting of three layer-cobalt, Alq_3 and nickel [38].

In order to investigate TMR in the SCJs, we switch the magnetization of FM layers in the centre of SCJ from parallel to antiparallel. For example, we change the magnetization of FM in both the 5th cell and the $(5+n+1)$th cell in $S(5,n)$. Now that we have already obtained the conductance of the SCJ with $S(5,n)$ in the parallel magnetic configuration (as shown in Figs. 2g–2i), we then calculate the conductance of corresponding SCJ in the antiparallel magnetic configuration (as shown in Figs. 4a–4c). It is obvious that compared with the parallel configuration, more conductance peaks appear in antiparallel configuration. And at some resonant wave vectors, the electrical conductance comes from the contribution of single spin state. Thereafter, the TMR in SCJs, which is given by equation (15), presents several interesting features (as shown in Figs. 4d–4f). (i) There exist several dips of TMR in the bandgap, and around each dip, inverse TMR is observed. Because the conductance in the antiparallel magnetic configuration is higher than that in the parallel configuration at some wave vectors in the SCJ, inverse TMR is definitely obtained at those wave vectors. (ii) Once the conductance peak in antiparallel magnetic configuration overlaps with that in parallel configuration, the dip of TMR is suppressed. (iii) With increasing n in the SCJ, large inverse TMR is obtained and more dips of inverse TMR is found. As we know, with increasing n, more and more conductance peaks appear and they are sharper in antiparallel configuration (as shown in Figs. 4a–4c), thereafter, multiple deep dips of inverse TMR appear in the bandgap in the SCJ. From this point of view, it is possible to use the SCJs to optimize the TMR and realize SC-based devices such as sensitive magnetic-field sensors.

The perfect transmission and inverse magnetoresistance in FM/SC cascade junctions described above is predicted to occur at zero temperature. At the finite temperature the presence of effects such as the inelastic scattering and phase breaking will destroy the coherent quantum interference [13,14], and hence the zero-temperature results will be smoothened [17]. Furthermore, the scatterings including momentum and spin scattering can lead to the broadening of the peaks [39]. This will decrease the efficiency of the spin filtering. The further investigation is undertaken.

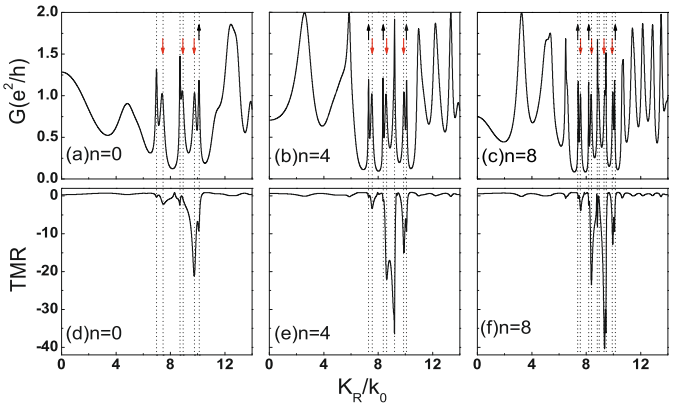

Fig. 4. (Color online) (a)–(c) The conductance (G) against the Rashba spin-orbit wave vector in the SCJ of $S(5,\ n)$ with different n, where the magnetization of FM in the central cell is reversed. (a) $n = 0$, (b) $n = 4$, and (c) $n = 8$. Here the arrow implies the conductance peak contributed by spin-up ($\uparrow$) or spin-down ($\downarrow$) electrons. And (d)–(f) TMR in the SCJ of $S(5,\ n)$ when the Rashba spin-orbit wave vector is varied: (d) $n = 0$, (e) $n = 4$, and (f) $n = 8$.

5 Summary

To summarize, we have investigated spin-dependent transport in FM/SC SCJs. Multiple perfect transmissions for spin-up or spin-down electrons have been found within the bandgap against the Rashba spin-orbit wave vector. For each spin state of electrons, the resonant wave vector and the mode number of resonant transmissions therein can be manipulated. Around resonant wave vector, spin polarization will be reversed, and fully spin-polarized conductance peaks can be observed. The resonant transmissions originate from the spin-dependent quasi-bound states at energies above the potential barriers, which are demonstrated by the electronic charge distributions in the system. If we change the magnetization of FM in the centre of the SCJ, inverse magnetoresistance can be observed. The investigations may be helpful in developing spin-dependent energy bandgap engineering and have potential applications in spin quantum devices.

This work was supported by grants from the National Natural Science Foundation of China (Grant Nos. 10625417, 10904061 and 10874068), the State Key Program for Basic Research from the Ministry of Science and Technology of China (Grant Nos. 2004CB619005 and 2006CB921804), and partly by Jiangsu Province (BK2008012).

References

1. S. Datta, B. Das, Appl. Phys. Lett. **56**, 665 (1990)
2. E.I. Rashba, Sov. Phys. Solid State **2**, 1190 (1960)
3. Y.A. Bychkov, E.I. Rashba, J. Phys. C **17**, 6039 (1984)
4. K.M. Jiang, Z.M. Zheng, B.G. Wang, D.Y. Xing, Appl. Phys. Lett. **89**, 012105 (2006)
5. J.L. Cheng, M.W. Wu, I.C. da Cunha Lima, Phys. Rev. B **75**, 205328 (2007)
6. J. Nitta, T. Akazaki, H. Takayanagi, T. Enoki, Phys. Rev. Lett. **78**, 1335 (1997)
7. D. Grundler, Phys. Rev. Lett. **84**, 6074 (2000)
8. L. Meier, G. Salis, I. Shorubalko, E. Gini, S. Schön, K. Ensslin, Nat. Phys. **3**, 650 (2007)
9. H. Ohno, Science **281**, 951 (1998)
10. E.I. Rashba, Phys. Rev. B **62**, R16267 (2000)
11. A.T. Hanbicki et al., Appl. Phys. Lett. **82**, 4092 (2003)
12. X. Jiang, R. Wang, R.M. Shelby, R.M. Macfarlane, S.R. Bank, J.S. Harris, S.S.P. Parkin, Phys. Rev. Lett. **94**, 056601 (2005)
13. Th. Schäpers, J. Nitta, H.B. Heersche, H. Takayanagi, Phys. Rev. B **64**, 125314 (2001)
14. F. Mireles, G. Kirczenow, Phys. Rev. B **66**, 214415 (2002)
15. Yong Guo, Xiao-Wei Yu, Yu-Xian Li, J. Appl. Phys. **98**, 053902 (2005)
16. R.L. Zhang, Z.J. Zhang, R.W. Peng, X. Wu, De Li, Jia Li, L.S. Cao, J. Appl. Phys. **103**, 07B727 (2008)
17. G. Papp, P. Vasilopoulos, F.M. Peeters, Phys. Rev. B **72**, 115315 (2005)
18. G. Papp, F.M. Peeters, J. Appl. Phys. **100**, 043707 (2006)
19. P. Földi, O. Kálmán, M.G. Benedict, F.M. Peeters, Phys. Rev. B **73**, 155325 (2006)
20. F. Capasso, C. Sirtori, J. Faist, D.L. Sivco, Sung-Nee G. Chu, A.Y. Cho, Nature **358**, 565 (1992)
21. P. Singha Deo, A.M. Jayannavar, Phys. Rev. B **50**, 11629 (1994)
22. G.J. Jin, Z.D. Wang, A. Hu, S.S. Jiang, J. Appl. Phys. **85**, 1597 (1999)
23. R.L. Zhang, R.W. Peng, L.S. Cao, Z. Wang, Z.H. Tang, X.F. Zhang, Mu Wang, A. Hu, Appl. Phys. Lett. **89**, 153114 (2006)
24. D.H. Dunlap, H-L. Wu, P.W. Phillips, Phys. Rev. Lett. **65**, 88 (1990)
25. V. Bellani, E. Diez, R. Hey, L. Toni, L. Tarricone, G.B. Parravicini, F. Domínguez-Adame, R. Gómez-Alcalá, Phys. Rev. Lett. **82**, 2159 (1999)
26. V. Pouthier, C. Girardet, Phys. Rev. B **66**, 115322 (2002)
27. Y.M. Liu, R.W. Peng, X.Q. Huang, Mu Wang, A. Hu, S.S. Jiang, Phys. Rev. B **67**, 205209 (2003)
28. R.W. Peng, Y.M. Liu, X.Q. Huang, F. Qiu, Mu Wang, A. Hu, S.S. Jiang, D. Feng, L.Z. Ouyang, J. Zou, Phys. Rev. B **69**, 165109 (2004)
29. Z. Zhao, F. Gao, R.W. Peng, L.S. Cao, D. Li, Z. Wang, X.P. Hao, Mu Wang, C. Ferrari, Phys. Rev. B **75**, 165117 (2007)
30. Y. Imry, R. Landauer, Rev. Mod. Phys. **71**, S306 (1999)
31. T.J. Thornton, Rep. Prog. Phys. **57**, 311 (1994)
32. C.M. Hu, T. Matsuyama, Phys. Rev. Lett. **87**, 066803 (2001)
33. M. Julliere, Phys. Lett. **54A**, 225 (1975)
34. J.M. De Teresa, A. Barthelemy, A. Fert, J.P. Contour, F. Montaigne, P. Sensor, Science **286**, 507 (1999)
35. S. Mukhopadhyay, I. Das, Phys. Rev. Lett. **96**, 026601 (2006)
36. J.S. Parker, P.G. Ivanov, D.M. Lind, P. Xiong, Y. Xin, Phys. Rev. B **69**, 220413(R) (2004)
37. J. Wang, X.C. Ma, Y. Qi, Y.S. Fu, S.H. Ji, Li Lu, J.F. Jia, Q.K. Xue, Appl. Phys. Lett. **90**, 113109 (2007)
38. S. Pramanik, S. Bandyopadhyay, K. Garre, M. Cahay, Phys. Rev. B **74**, 235329 (2006)
39. M.Q. Weng, M.W. Wu, L. Jiang, Phys. Rev. B **69**, 245320 (2004)